

# Effect of Gas Composition on Temperature and CO<sub>2</sub> Conversion in a Gliding Arc Plasmatron reactor: Insights for Post-Plasma Catalysis from Experiments and Computation

Wencong Xu<sup>+, [a, b, c]</sup> Senne Van Alphen<sup>+, [b]</sup> Vladimir V. Galvita,<sup>[c]</sup> Vera Meynen,<sup>[a]</sup> and Annemie Bogaerts<sup>\*[b]</sup>

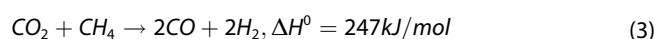
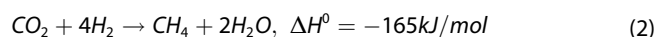
Plasma-based CO<sub>2</sub> conversion has attracted increasing interest. However, to understand the impact of plasma operation on post-plasma processes, we studied the effect of adding N<sub>2</sub>, N<sub>2</sub>/CH<sub>4</sub> and N<sub>2</sub>/CH<sub>4</sub>/H<sub>2</sub>O to a CO<sub>2</sub> gliding arc plasmatron (GAP) to obtain valuable insights into their impact on exhaust stream composition and temperature, which will serve as feed gas and heat for post-plasma catalysis (PPC). Adding N<sub>2</sub> improves the CO<sub>2</sub> conversion from 4% to 13%, and CH<sub>4</sub> addition further promotes it to 44%, and even to 61% at lower gas flow rate (6 L/min), allowing a higher yield of CO and hydrogen for PPC.

The addition of H<sub>2</sub>O, however, reduces the CO<sub>2</sub> conversion from 55% to 22%, but it also lowers the energy cost, from 5.8 to 3 kJ/L. Regarding the temperature at 4.9 cm post-plasma, N<sub>2</sub> addition increases the temperature, while the CO<sub>2</sub>/CH<sub>4</sub> ratio has no significant effect on temperature. We also calculated the temperature distribution with computational fluid dynamics simulations. The obtained temperature profiles (both experimental and calculated) show a decreasing trend with distance to the exhaust and provide insights in where to position a PPC bed.

## Introduction

In the past decades, accumulating evidence has demonstrated that the increasing emission of greenhouse gases is leading to global warming.<sup>[1]</sup> Specifically, the concentration of CO<sub>2</sub> in the atmosphere has risen significantly, surging from 362 ppm at the end of the last century to 420 ppm in June 2023, based on the data from the "National Oceanic and Atmospheric Administration (NOAA) Global Monitoring Laboratory".<sup>[2]</sup> Therefore, numerous techniques are being developed to capture CO<sub>2</sub> and convert it into value-added fuels or chemical products.<sup>[3–7]</sup> Several different chemical processes, including CO<sub>2</sub> splitting (Eq. (1)), CO<sub>2</sub> methanation with H<sub>2</sub> (Eq. (2)), and CO<sub>2</sub> dry reforming of methane (DRM) Eq. (3), have been investigated for the conversion of CO<sub>2</sub> either directly or in combination with other molecules like CH<sub>4</sub>, H<sub>2</sub>, or/and H<sub>2</sub>O.<sup>[8–10]</sup> However, as a relatively stable molecule, the activation of CO<sub>2</sub> remains a

significant challenge for many (catalytic) reactions. Thermally, direct CO<sub>2</sub> splitting is energy-consuming and only favorable at high temperature. For instance, at 2000 K, it is estimated that, to achieve a CO<sub>2</sub> conversion of 1.5%, the energy cost (EC) will be about 7.9 MJ/mol and the final energy efficiency (EE) is just 4.4%.<sup>[11]</sup>



In recent years, plasma technology has been widely applied in CO<sub>2</sub> conversion because it can activate the gas molecules by electron impact excitation, ionization and dissociation via electrical energy supply. This creates excited species, ions and radicals that can form new molecules.<sup>[11,12]</sup> Compared with conventional thermal approaches, electrical energy is transferred to the gas, making it a promising technology for the ongoing energy transition in chemical production.<sup>[13–18]</sup> Furthermore, plasma can be integrated with catalysts to create a hybrid plasma-catalysis process, which holds promise for enhancing CO<sub>2</sub> conversion, improving energy efficiency and chemical product selectivity.<sup>[15,19–21]</sup> A lot of research on CO<sub>2</sub> conversion is performed with various kinds of plasmas, including a dielectric barrier discharge (DBD),<sup>[22]</sup> microwave (MW),<sup>[23]</sup> spark or gliding arc (GA) discharge.<sup>[12,24]</sup> Among these plasma techniques, gliding arc plasma is promising, because it can typically produce electrons with mean energy around 1 eV, which is ideal to activate CO<sub>2</sub>.<sup>[12,25]</sup> Moreover, the GA creates heat in the plasma zone, with temperatures up to a few 1000 K,<sup>[26,27]</sup> which influences the reactions and allows for post-plasma catalysis in

[a] W. Xu,<sup>+</sup> Prof. V. Meynen  
Department of Chemistry, Research group LADCA  
University of Antwerp  
Universiteitsplein 1, B-2610 Wilrijk, Antwerp, Belgium

[b] W. Xu,<sup>+</sup> S. Van Alphen,<sup>+</sup> Prof. A. Bogaerts  
Department of Chemistry, Research group PLASMANT  
University of Antwerp  
Universiteitsplein 1, B-2610 Wilrijk, Antwerp, Belgium  
E-mail: annemie.bogaerts@uantwerpen.be

[c] W. Xu,<sup>+</sup> Prof. V. V. Galvita  
Department of Materials, Textiles and Chemical Engineering, Research group LCT  
Ghent University  
Technologiepark 125, B-9052, Ghent, Belgium

[<sup>+</sup>] The authors equally contributed to this work

Supporting information for this article is available on the WWW under <https://doi.org/10.1002/cssc.202400169>

the exhaust stream of the plasma reactor, recovering (at least part of) the heat of the plasma process.<sup>[14,28]</sup>

Several different types of GA plasmas have been designed, e.g. classical 2D GA,<sup>[29]</sup> 3D rotating gliding arc (RGA),<sup>[30,31]</sup> 3D gliding arc plasmatron (GAP),<sup>[12]</sup> and dual-vortex plasmatron (DVP).<sup>[27]</sup> The classical 2D GA plasma is widely studied, however, it exhibits some drawbacks, as it is incompatible with industrial application because of its 2D flat electrodes. Furthermore, not all the gas passes through the arc, and thus it is not fully activated. Finally, a relatively high gas flow rate is needed to sustain the arc gliding process, which gives rise to a short gas residence time in the plasma. To overcome these problems, several 3D gliding arc plasma reactor designs have been developed over the years, in which the gas flows tangentially into the reactor, forming a stable vortex gas flow.<sup>[12,30,32]</sup> Furthermore, recently, a novel DVP reactor was designed and tested, enabling to separate the arc into two directions with longer residence time and highly turbulent flow.<sup>[27]</sup> These 3D GA reactors are also characterized by high flow rates, but the mechanism to sustain the arc gliding mechanism is different from 2D GA reactors, with typically a cylindrical arc column along the reactor axis, giving rise to a longer gas residence time in the plasma.

Ramakers et al. studied the conversion of CO<sub>2</sub> in the GAP reactor, yielding as highest CO<sub>2</sub> conversion 8.6% and an energy efficiency EE of 30% at an energy cost EC of 39 kJ/L.<sup>[12]</sup> The group PLASMANT also investigated DRM in the GAP, achieving absolute CO<sub>2</sub> and CH<sub>4</sub> conversions of about 24% and 42%, or effective conversions of about 18% and 10%, respectively, at a CH<sub>4</sub> fraction of 25% in the gas flow, corresponding to an EC of 10 kJ/L and an EE of 66%.<sup>[24]</sup> In a later study, the same group reported DRM upon addition of N<sub>2</sub> and O<sub>2</sub> in the same GAP reactor, and obtained absolute CO<sub>2</sub> conversions between 31% and 52%, and CH<sub>4</sub> conversions between 55 and 99%, corresponding to a total EC of 13–20 kJ/L (or 3.4–5.0 eV/molec), depending on the gas mixture.<sup>[33]</sup> Recently, the addition of only N<sub>2</sub> on the DRM process was studied, and it was found that 20% N<sub>2</sub> addition yields CO<sub>2</sub> and CH<sub>4</sub> absolute conversions of 29 and 36%. However, these values rise notably upon N<sub>2</sub> addition, up to 48% for CO<sub>2</sub> and 61% for CH<sub>4</sub> at 80% N<sub>2</sub>.<sup>[34]</sup>

To fully make use of the heat produced by the GA plasma, research has been focused on establishing synergistic effects of heterogeneous catalysis in combination with the plasma. Zhang et al. reported a combination of a GA plasma with a post-plasma TiO<sub>2</sub> bed for CO<sub>2</sub> splitting.<sup>[35]</sup> Simulation of the addition of the post-plasma catalyst bed indicated that a strong back-flow was formed and experiments confirmed an enhancement in reaction performance. Notably, when the distance between the plasma reactor outlet and the catalyst bed was only 5 mm, fluctuations in CO<sub>2</sub> conversion and EE occurred at flow rates lower than 4 L/min. A synergistic effect was observed because the presence of TiO<sub>2</sub> enhanced the CO<sub>2</sub> conversion from 4.6 to 10.8% and the EE from 5.4 to 12.6% at a gas flow rate of 2 L/min. In another study, 25% increase of CH<sub>4</sub> conversion, 20% increase of CO<sub>2</sub> conversion, around 30% increase in H<sub>2</sub> yield and about 22% increase in EE were achieved when combining a NiO/Al<sub>2</sub>O<sub>3</sub> catalyst post-plasma with a GA plasma in DRM.<sup>[36]</sup>

Significant improvements were obtained when a GA plasma was combined with a Ni/CeO<sub>2</sub>/Al<sub>2</sub>O<sub>3</sub> catalyst post-plasma and extra heating was supplied to the catalyst by a tubular furnace.<sup>[37]</sup> When there was no extra heating, the performance of the plasma with catalyst was almost the same as the plasma alone. This could be explained because of the low temperature (around 300–500 °C) of the plasma gas effluent, at which range the catalyst was inactive for DRM. When the tubular furnace was heated, the combined effect of plasma and catalyst resulted in an increase in CO<sub>2</sub> and CH<sub>4</sub> conversion, from about 25% and 39% in plasma alone, and 62% and 46% in thermal catalysis, to 70% and 59% in the case of plasma catalysis with heating, respectively. Hence, the temperature at the outlet of the plasma GAP reactor is important when combining it with a post-plasma catalytic bed. Nevertheless, to our knowledge, little literature reported on the variation of temperature after plasma in relation to the gas composition used.

In this paper, we employed a GAP setup, which was reported before,<sup>[38]</sup> to investigate the impact of additives such as N<sub>2</sub>, CH<sub>4</sub>, and H<sub>2</sub>O vapor on the CO<sub>2</sub> conversion. We aim to provide suggestions for selecting optimal conditions for enhanced CO<sub>2</sub> conversion. Moreover, we recorded the temperature after the plasma, offering insights in where to position the catalyst in a post-plasma catalysis (PPC) system. Additionally, we performed simulations to analyze the temperature distribution within the GAP reactor and post-plasma reactor tube, providing a potential view for designing post-plasma catalysis systems.

## Results and Discussion

### CO<sub>2</sub> and CH<sub>4</sub> Conversion

To quantify the CO<sub>2</sub> and CH<sub>4</sub> conversions, the absolute and effective conversions of these two gases were defined. The absolute conversion (Figure 1, solid lines), or simply called “conversion”, gives a direct comparison between the different configurations, while the effective conversion (Figure 1, dash lines) considers the dilution of CO<sub>2</sub> or CO<sub>2</sub>/CH<sub>4</sub> in N<sub>2</sub>, which is relevant for application and economics as this dilutes and thus limits the products formed.

Figure 1 presents the conversions of CO<sub>2</sub> and CH<sub>4</sub> in different gas mixtures. In the CO<sub>2</sub>/N<sub>2</sub> gas composition, a significant increase in absolute conversion of CO<sub>2</sub> is observed when N<sub>2</sub> was added into CO<sub>2</sub> from 0% to 80%, as shown in Figure 1A. The value especially increases significantly when the N<sub>2</sub> fraction rises from 60% to 80%. A maximum absolute conversion of 13% was obtained for a N<sub>2</sub> fraction of 80%. Therefore, N<sub>2</sub> in the feed gas is beneficial for converting CO<sub>2</sub>. The reason for this was explained already in literature: the CO<sub>2</sub> conversion in a GAP is most effective through the vibrational levels and the high N<sub>2</sub> vibrational levels help to populate the CO<sub>2</sub> vibrational levels.<sup>[38]</sup> It is interesting to note that at N<sub>2</sub> fractions of 50% and 60%, the CO<sub>2</sub> absolute conversion remained almost the same. This trend is similar as the trend in temperature (Figure 6A) at N<sub>2</sub> fraction of 50% and 60%. On the

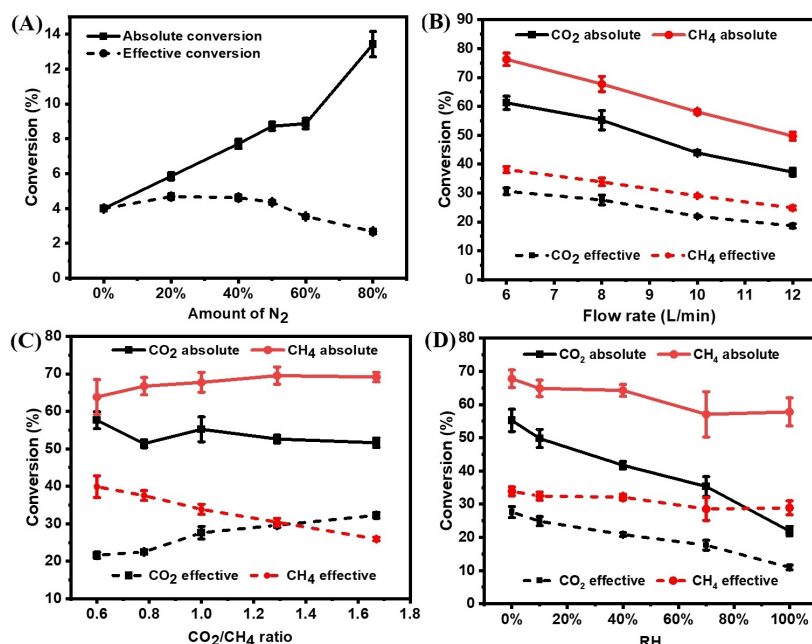


**Figure 1.** Conversion of CO<sub>2</sub> and CH<sub>4</sub> as a function of gas composition, gas flow rate and relative humidity (RH). (A) CO<sub>2</sub> conversion in CO<sub>2</sub>/N<sub>2</sub> mixture: Total gas flow rate = 10 L/min, N<sub>2</sub> fraction varying from 0% to 80%. (B–D) CO<sub>2</sub> and CH<sub>4</sub> conversion in CO<sub>2</sub>/CH<sub>4</sub>/N<sub>2</sub> mixture (B,C), and with H<sub>2</sub>O addition (D): (B) Total gas flow rate varied from 6 to 12 L/min, CO<sub>2</sub>/CH<sub>4</sub>/N<sub>2</sub> = 1/1/8. (C) Total gas flow rate = 8 L/min, N<sub>2</sub> = 6.4 L/min, CO<sub>2</sub>/CH<sub>4</sub> ratio varied between 0.6 and 1.67. (D) Total gas flow rate = 8 L/min, CO<sub>2</sub>/CH<sub>4</sub>/N<sub>2</sub> = 1/1/8, H<sub>2</sub>O amount varied between 0% and 100% RH.

one hand, N<sub>2</sub> is contributing to the CO<sub>2</sub> conversion, by collisions between vibrationally or electronically excited levels of N<sub>2</sub>, which help in the dissociation of CO<sub>2</sub>, but the effect of course becomes relatively less pronounced at higher N<sub>2</sub> fractions. On the other hand, the CO<sub>2</sub> conversion also rises upon higher temperature, as the conversion proceeds mainly by thermal chemistry, and because the temperature does not increase in this range (cf. Figure 6A), the CO<sub>2</sub> conversion also stays constant. Moreover, at N<sub>2</sub> fractions above 60%, the CO<sub>2</sub> conversion increased much more. The temperature data, as shown in Figure 6A, shows a similar trend. It seems that the N<sub>2</sub> promotion effect at fractions below 50% is weaker than at fractions above 60%. For the fraction between 50% and 60%, a combined effect results in the CO<sub>2</sub> conversion and gas temperature remaining almost the same, which is probably because the energy transfer from N<sub>2</sub>, which increases the gas temperature (the mechanism for it is explained in the followed temperature part), compensates the energy needed for the rise in CO<sub>2</sub> conversion.

For the effective conversion of CO<sub>2</sub>, however, because of the decreasing CO<sub>2</sub> fraction in the mixture, the effective conversion of CO<sub>2</sub> shows the opposite trend, with first a slight increase from 4% to 4.7% up to 20% N<sub>2</sub> fraction, and then a drop to 2.7% with increasing N<sub>2</sub> fraction. As the N<sub>2</sub> fraction is lower than 50%, the increase in absolute CO<sub>2</sub> conversion can, to some extent, compensate for the lower concentration of CO<sub>2</sub>, but with a higher N<sub>2</sub> fraction, the rise in conversion is not enough to compensate for the drop in CO<sub>2</sub> conversion.<sup>[38]</sup>

At the same gas flow rate of 10 L/min, once CH<sub>4</sub> is added into the mixture (Figure 1B), the absolute conversion of CO<sub>2</sub> increases to 43%, more than three times the maximum value in

the CO<sub>2</sub>/N<sub>2</sub> mixture. Moreover, the conversion of CO<sub>2</sub> increases upon decreasing gas flow rate, reaching its highest value of 61% at a flow rate of 6 L/min. The reason that the highest conversion is obtained at the lowest flow rate is due to the longer residence time, giving sufficient time for more gas molecules to react in the plasma region. It should be noticed that when the gas flow rate was increased from 6 L/min to 12 L/min, the pressure of the inlet gas also increased a bit, as measured by the pressure gauge, shown in the Supporting Information; see experimental section, Figure S1. Furthermore, at higher flow rates (e.g., 14 L/min), plasma ignition was very difficult, and the plasma arc became unstable. Besides this, the conversion of CH<sub>4</sub> is always higher than that of CO<sub>2</sub> because the energy needed for the plasma-based decomposition of CH<sub>4</sub> is lower than that for CO<sub>2</sub>, due to the lower bond strength to break the C–H vs C=O bond (i.e., 4.48 eV vs 5.52 eV).<sup>[33]</sup> Since the ratio of CO<sub>2</sub>/CH<sub>4</sub> did not change in Figure 1B, the effective conversions of both CO<sub>2</sub> and CH<sub>4</sub> show the same trend as the absolute conversions, but the values are obviously lower. As shown in Figure 2B, although a higher CO<sub>2</sub> conversion was obtained at lower flow rates, the cathode can be seriously damaged. Therefore, we used a gas flow rate of 8 L/min, at which the cathode was safe, to study how the CO<sub>2</sub>/CH<sub>4</sub> ratio affects the conversion results.

Figure 1C illustrates that a higher CO<sub>2</sub>/CH<sub>4</sub> ratio slightly increases the absolute conversion of CH<sub>4</sub> from 64% to 69%, while the conversion of CO<sub>2</sub> first decreases a bit from about 58% (CO<sub>2</sub>/CH<sub>4</sub> ratio of 0.6) to 51% (CO<sub>2</sub>/CH<sub>4</sub> ratio of 0.78) and then stays generally constant. However, different from the absolute conversion, the effective conversion of CH<sub>4</sub> decreases significantly from 40% to 26% as the CO<sub>2</sub> fraction increases,

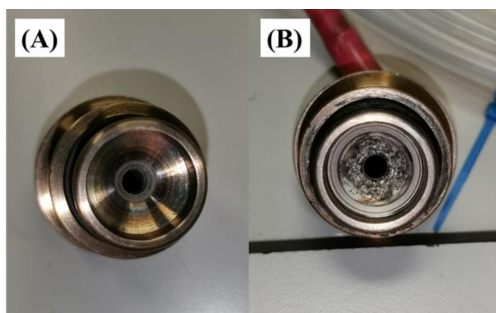


**Figure 2.** Photographs of (A) clean reactor cathode, and (B) after reaction with a gas flow rate of 6 L/min, indicating clear damage of the cathode.

while the CO<sub>2</sub> effective conversion shows an obvious increase from 22% to 32%. These conversion values are in line with previous results obtained for the GAP in CO<sub>2</sub>/CH<sub>4</sub>/N<sub>2</sub> mixtures,<sup>[34]</sup> but they give additional insights into how to adjust the CO<sub>2</sub>/CH<sub>4</sub> ratio for achieving better results.

For the PPC system, the outlet gas of the plasma will be utilized as the feed gas for the catalyst to further convert the unreacted reactants or the products from the plasma. This catalyst is a thermal catalyst, which will possibly suffer from deactivation due to coke deposition. Addition of H<sub>2</sub>O can help to decrease the formation of solid carbon, as well as produce more H<sub>2</sub>.<sup>[39]</sup> Therefore, we also added H<sub>2</sub>O into the feed gas. Compared with DRM without water, adding water causes a serious drop in the absolute conversion of CO<sub>2</sub>, from 55% to 22% for a RH ranging from 0% to 100% (Figure 1D). This is attributed to the drop in electron density, as water is trapping the electrons.<sup>[39]</sup> Another reason is probably that the OH radicals produced by water splitting react with CO, forming CO<sub>2</sub> again, as revealed by detailed chemical kinetics modeling for DBD plasma, where a similar effect was observed.<sup>[40]</sup> The CH<sub>4</sub> conversion decreases less, from 68% to 58%. The effective conversions of CO<sub>2</sub> and CH<sub>4</sub> show the same, but less significant decreasing tendency. This is different from literature, where it was reported that the CH<sub>4</sub> conversion increases as the molar ratio of H<sub>2</sub>O molecules to carbon atoms increases from 0 to 0.58.<sup>[39]</sup> This may be due to the difference in CO<sub>2</sub>/CH<sub>4</sub> ratio. They used a 1.5 times higher ratio than what we used (ratio of 1).

### Products Selectivity and H<sub>2</sub>/CO Ratio

As is clear from Figure 3A, the selectivities of CO and H<sub>2</sub> both increase slightly upon increasing gas flow rate, from 68% to 75%, and from 80% to 85%, respectively. In contrast, the selectivity of C<sub>2</sub>H<sub>2</sub> first drops from 22 to 18%, and then remains constant around 19% upon higher gas flow rates. The H<sub>2</sub>/CO ratio shows a similar trend, as it decreases firstly from 1.6 to 1.5 and then remains constant at a ratio of 1.4.

As the CO<sub>2</sub>/CH<sub>4</sub> ratio increases from 0.6 to 1.67, the selectivity of CO keeps increasing from 45% to 93%, while the selectivity of H<sub>2</sub> remains at a high level above 81% and fluctuates around 90%, and the selectivity of C<sub>2</sub>H<sub>2</sub> decreases from 31 to 11% (Figure 3B). In previous research with the

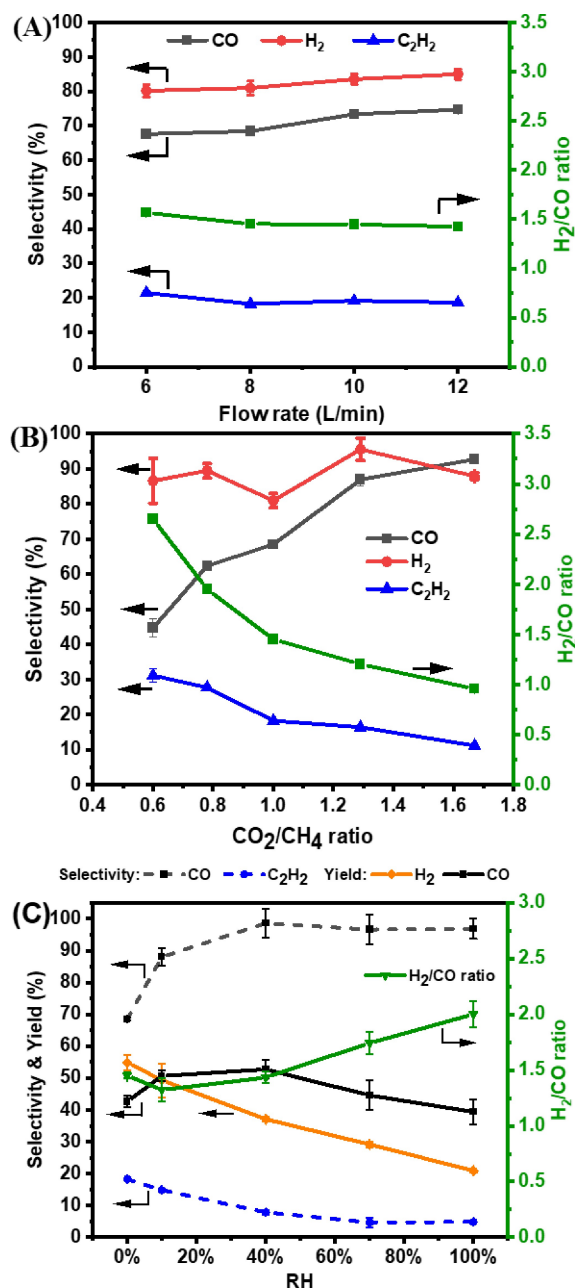


**Figure 3.** (A, B) Selectivity of CO, H<sub>2</sub>, C<sub>2</sub>H<sub>2</sub> (left y-axes) and H<sub>2</sub>/CO ratio (green curves, right y-axes), and © selectivity of CO and C<sub>2</sub>H<sub>2</sub> (dashed lines, left y-axis), yield of H<sub>2</sub> and CO (solid lines, left y-axis) and H<sub>2</sub>/CO ratio (right y-axis), as a function of gas flow rate (A), gas composition (B) and RH (C). (A) The total gas flow rate varied from 6 to 12 L/min, CO<sub>2</sub>/CH<sub>4</sub>/N<sub>2</sub> = 1/1/8. (B) Total gas flow rate = 8 L/min, N<sub>2</sub> = 6.4 L/min, CO<sub>2</sub>/CH<sub>4</sub> ratio varied between 0.6 and 1.67. (C) Total gas flow rate = 8 L/min, CO<sub>2</sub>/CH<sub>4</sub>/N<sub>2</sub> = 1/1/8, the H<sub>2</sub>O amount varied between 0% and 100% RH.

GAP,<sup>[34]</sup> a constant CO<sub>2</sub>/CH<sub>4</sub> ratio of 1 was used, and the focus was on the optimal effective conversion and EC, which were achieved with 20% N<sub>2</sub>. However, the CO and H<sub>2</sub> selectivities were almost the lowest at this N<sub>2</sub> fraction, compared with other N<sub>2</sub> fractions. Our results indicate that these selectivities may be enhanced by increasing the CO<sub>2</sub>/CH<sub>4</sub> ratio.

Figure 4 compares photographs of the post-plasma reactor tube when using CO<sub>2</sub>/CH<sub>4</sub> ratios of 0.6 and 1.67. With higher

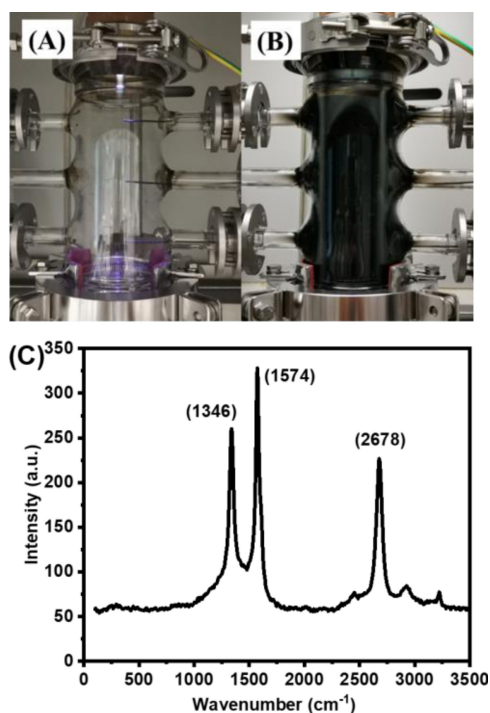


**Figure 4.** Photographs of post-plasma reactor tube and the Raman spectrum of the solid carbon product collected from the GAP DRM in the (B) case, at a total gas flow rate of 8 L/min,  $N_2 = 6.4$  L/min, for (A)  $CO_2/CH_4 = 1.67$ , (B)  $CO_2/CH_4 = 0.6$ , (C) Raman spectrum of carbon collected in the (B) case.

$CO_2$  fraction, there was no visible carbon deposition on the inside wall of reactor (Figure 4A), while serious carbon deposition was visible when more  $CH_4$  was added into the feed gas (Figure 4B). We believe this is because the carbon produced from methane ( $CH_4 \rightarrow C + 2H_2$ ,  $\Delta H^0 = 75.6$  kJ/mol) reacts directly with  $CO_2$  or with the oxygen atom produced by  $CO_2$ , promoting the CO production. Indeed, such reactions were demonstrated to happen also when placing a carbon bed after the GAP plasma reactor, as demonstrated by detailed chemistry modeling.<sup>[41]</sup> This also explains why the  $C_2H_2$  selectivity decreases, as more C atoms recombine with O atoms to form CO rather than  $C_2H_2$ . Raman spectroscopy, as shown in Figure 4C, was employed to analyze the composition of the carbon on the reactor's inner wall. Distinct carbon signals were detected at around  $1346\text{ cm}^{-1}$  (D band) and  $1574\text{ cm}^{-1}$  (G band), with an  $I_D/I_G$  value of 0.79. The D band appears due to the defects of the product, and the G band reflects the in-plane  $sp^2$  carbon vibrations. The value of  $I_D/I_G$  is used to evaluate the defects of the product: the larger the value, the smaller the size of the product.<sup>[18,42]</sup> Additionally, a 2D band at  $2678\text{ cm}^{-1}$  was observed, which is typically attributed to the overtone of the D band.<sup>[18]</sup> Although the conversions of  $CO_2$  and  $CH_4$  change only slightly for different  $CO_2/CH_4$  ratios, relatively more  $H_2$  is produced than CO at lower  $CO_2/CH_4$  ratio, creating a maximum  $H_2/CO$  ratio of 2.7. This is interesting for further use of the syngas via Fischer-Tropsch synthesis, for example, to produce methanol, for which the ideal  $H_2/CO$  ratio is equal to 2.<sup>[43]</sup>

The selectivity of CO increases significantly once  $H_2O$  was added into the feed gas (Figure 3C), although the conversion

decreases (Figure 1D) due to the water-gas shift reaction (WGSR) ( $CO + H_2O \rightarrow CO_2 + H_2$ ,  $\Delta H^0 = -42.1$  kJ/mol). This can be explained by the higher number of O atoms produced from the  $H_2O$  molecules, enhancing the oxidation of carbon-containing species (deposited carbon or hydrocarbon species) into CO. This results in the general increasing trend of CO selectivity. Vice versa, the  $C_2H_2$  selectivity decreases upon  $H_2O$  addition. Literature reported that the formation of hydrocarbons was strongly affected by the decomposition of  $CH_4$  into  $CH_3$ ,  $CH_2$ , and CH. The addition of  $H_2O$  limited the formation of CH, which was proven by optical emission spectrometry,<sup>[39]</sup> leading to less  $C_2H_2$  formation. Although the outlet water was collected, it was impossible to precisely estimate how much water participated in the reaction, because part of the water condensed and adhered on the walls of the cooling device. Therefore, it was difficult to calculate the  $H_2$  selectivity in a reliable way in this system and the values will not be used here. Upon increasing RH from 10% to 100%, the yield of  $H_2$  exhibited a decrease, as a lot of the  $H_2O$  was not involved in the plasma reaction. However, the relative amount of  $H_2$  produced increased with addition of  $H_2O$ . As shown in Figure 3C (green line), the  $H_2/CO$  ratio drops at first for 10% RH and then increases with increasing amount of  $H_2O$ . This is because at low RH, the CO amount increases more than that of  $H_2$ , leading to a slight decrease of the ratio. As the RH further increases, the  $H_2$  amount continues to increase, while the CO amount already reached its maximum at 40% RH.

### Specific Energy Input and Energy Cost

Figure 5 illustrates the specific energy input (SEI) and energy cost (EC) for the various conditions investigated. When only  $N_2/CO_2$  was used for the plasma reaction, the SEI fluctuated between 1.3 and 1.7 kJ/L (Figure 5A), suggesting that the changes of the gas composition had only small effect on the value of the SEI, as the current was fixed and the power changed only little with gas composition. Different from the SEI, the EC generally exhibits an increasing tendency. With pure  $CO_2$ , the EC is 17.1 kJ/L. This value decreases slightly to 15.1 kJ/L as the fraction of  $N_2$  increases to 20%. It rises however to 36.1 kJ/L at a higher  $N_2$  fraction of 40%, fluctuates around this value up to 60%  $N_2$  and then increases to 48 kJ/L with 80%  $N_2$  used. This is directly correlated to the lower effective  $CO_2$  conversion upon higher  $N_2$  fraction, and is most likely due to the higher fraction of energy used to activate the  $N_2$  molecules rather than  $CO_2$ .

When increasing the gas flow rate and keeping the gas ratio of  $CO_2/CH_4/N_2$  at 1/1/8 (Figure 5B), the SEI decreases linearly, which is logical, as the SEI is inversely proportional to the gas flow rate (see Supporting Information, Eq. S5). However, the EC fluctuates between 5.6 and 6.2 kJ/L, with a maximum value at a gas flow rate of 6 L/min. As the EC is relatively stable, the gas flow rate seems to have little effect on the energy needed for molecules to be converted. More or less the same can be concluded about the effect of the  $CO_2/CH_4$  ratio, because the SEI and EC steadily decrease only from 3.7 to 3.2 kJ/L and from

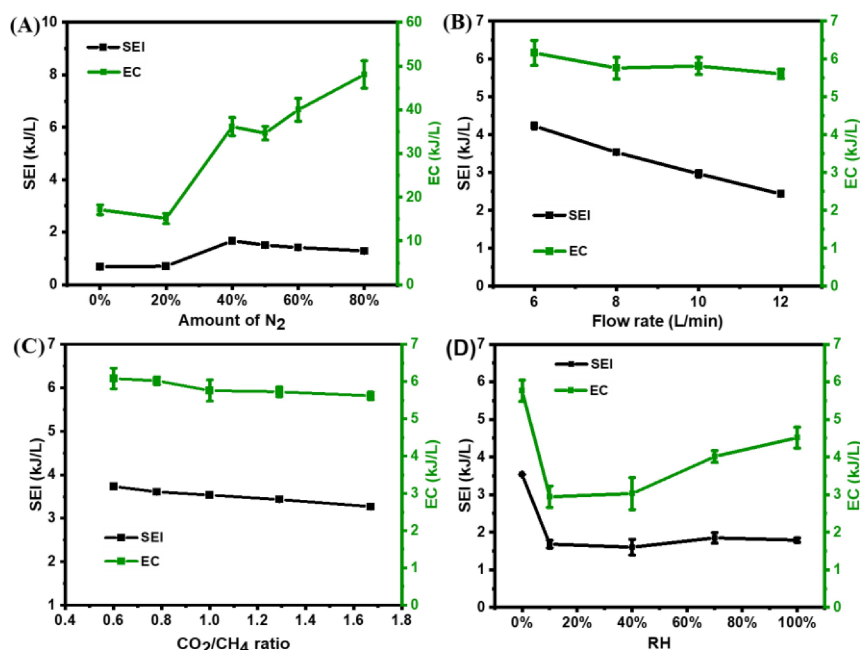


**Figure 5.** SEI and EC as a function of gas composition, gas flow rate and RH. (A) Total gas flow rate = 10 L/min, N<sub>2</sub> fraction in CO<sub>2</sub> varied from 0% to 80%. (B) The total gas flow rate varied from 6 to 12 L/min, CO<sub>2</sub>/CH<sub>4</sub>/N<sub>2</sub> = 1/1/8. (C) Total gas flow rate = 8 L/min, N<sub>2</sub> = 6.4 L/min, CO<sub>2</sub>/CH<sub>4</sub> ratio varied between 0.6 and 1.67. (D) Total gas flow rate = 8 L/min, CO<sub>2</sub>/CH<sub>4</sub>/N<sub>2</sub> = 1/1/8, H<sub>2</sub>O amount varied between 0% and 100% RH.

6.1 to 5.6 kJ/L, upon increasing the CO<sub>2</sub>/CH<sub>4</sub> ratio (Figure 5C). The effect of different N<sub>2</sub> contents on the EC for DRM, at a CO<sub>2</sub>/CH<sub>4</sub> ratio of 1, was also studied in,<sup>[34]</sup> and 20% N<sub>2</sub> addition yielded the lowest EC, in line with our results (Figure 5A). Moreover, the EC can be further slightly reduced by increasing the CO<sub>2</sub>/CH<sub>4</sub> ratio, as indicated by our results (Figure 5C).

When H<sub>2</sub>O is added, the SEI and EC show similar trends (Figure 5D): they decline significantly from 3.5 kJ/L and 5.8 kJ/L to 1.7 kJ/L and 2.9 kJ/L for 10% RH, followed by an increase to 1.9 kJ/L and 4 kJ/L, for 70% RH. Finally, a small decrease in SEI to 1.8 kJ/L but a slightly higher EC of 4.5 kJ/L is observed with 100% RH. Generally, the introduction of H<sub>2</sub>O thus results in a lower SEI and EC for the conversion.

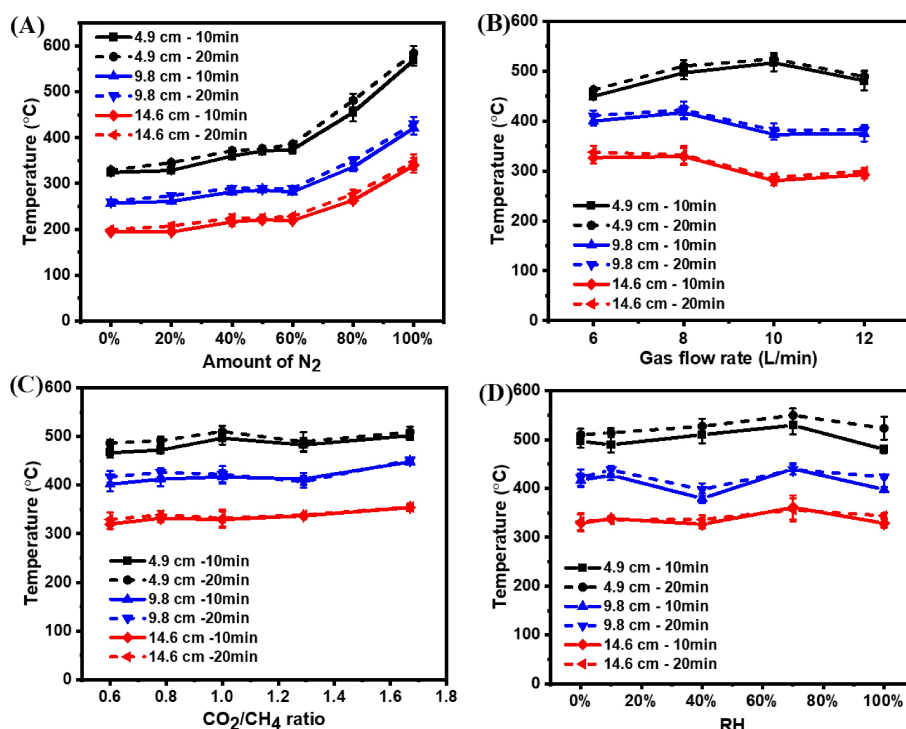
### Temperature After the Plasma

Figure 6 illustrates the measured post-plasma temperature, at three different distances from the plasma exhaust, for all conditions investigated. All experiments were repeated at least three times, and the detailed temperature data as a function of time, as well as more detailed information, are presented in Figure S3–6. The following conclusions can be drawn from Figure S3–6: (1) The more CO<sub>2</sub> in the N<sub>2</sub>/CO<sub>2</sub> system, the more stable is the temperatures measured after plasma, suggesting that CO<sub>2</sub> is beneficial for giving a stable plasma flame. The reason that N<sub>2</sub> addition increases the gas temperature is that the N<sub>2</sub> molecules can acquire energy from the plasma, most of which cannot be used for chemical reaction due to the strong triple bond of N<sub>2</sub>, and it can only be vibrationally excited, after which the vibrational levels eventually relax their acquired

energy, increasing the gas temperature.<sup>[34]</sup> (2) Adding CH<sub>4</sub> into the N<sub>2</sub>/CO<sub>2</sub> system results in an unstable plasma flame but a generally stable temperature at the same position after plasma. (3) Addition of H<sub>2</sub>O (RH ≥ 40%) makes the plasma flame unstable in the first 10 minutes, resulting in a sudden decrease in temperature. This could be due to condensed H<sub>2</sub>O inside the cathode, formed during the flushing time.

The temperatures after 10 and 20 minutes of plasma operation at all different conditions are summarized in Figure 6. When N<sub>2</sub> is added into CO<sub>2</sub> (Figure 6A), the temperatures increase at all three distances from the plasma exhaust. As the N<sub>2</sub> fraction increases, the temperature at 4.9 cm increases significantly from 324 °C with pure CO<sub>2</sub> to 569 °C with pure N<sub>2</sub>. Although relatively stable in temperature up to 60% N<sub>2</sub>, a sharp increase happens when the N<sub>2</sub> concentration is over 60%. Moreover, the temperatures at 10 and 20 minutes are almost the same, suggesting that the temperature was stable after 10 minutes plasma, which was also proven by the data in Figure S3.

Upon adding CH<sub>4</sub> into the CO<sub>2</sub>/N<sub>2</sub> mixture and fixing the gas ratio of CO<sub>2</sub>/CH<sub>4</sub> to 1 (Figure 6B), the temperature at 4.9 cm first increases upon rising gas flow rate, reaching a maximum value of 516 °C at 10 L/min and then it drops to 481 °C at 12 L/min. However, different from the CO<sub>2</sub>/N<sub>2</sub> system, in which the temperature at 9.8 cm and 14.6 cm showed the same trends as at 4.9 cm, the temperature at lower position (9.8 cm) now drops from 417 °C at 8 L/min to 373 °C at 10 L/min, while at 14.6 cm it drops from about 330 °C at 8 L/min to 280 °C at 10 L/min. The lowest temperature at a distance of 9.8 cm and 14.6 cm was measured at a gas flow rate of 10 L/min. The higher temperature might have contributed to the higher conversions of CO<sub>2</sub>



**Figure 6.** Temperature at 4.9 cm, 9.8 cm, and 14.6 cm after the plasma reactor, for 10 min and 20 min plasma operation, as a function of gas composition, gas flow rate and RH. (A) Total gas flow rate = 10 L/min, N<sub>2</sub> fraction in CO<sub>2</sub> varied from 0% to 100%. (B) The total gas flow rate varied from 6 to 12 L/min, CO<sub>2</sub>/CH<sub>4</sub>/N<sub>2</sub> = 1/1/8. (C) Total gas flow rate = 8 L/min, N<sub>2</sub> = 6.4 L/min, CO<sub>2</sub>/CH<sub>4</sub> ratio varied between 0.6 and 1.67. (D) Total gas flow rate = 8 L/min, CO<sub>2</sub>/CH<sub>4</sub>/N<sub>2</sub> = 1/1/8, H<sub>2</sub>O amount varied between 0% and 100% RH.

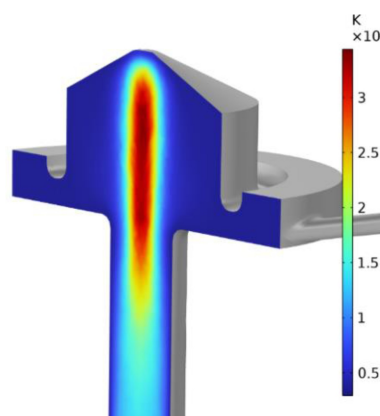
and CH<sub>4</sub> as the dry reforming reaction is endothermic. Besides this, as shown in Figure 2B, the cathode melted at 6 L/min, suggesting a higher gas flow rate is necessary.

At fixed gas flow rate, changing the CO<sub>2</sub>/CH<sub>4</sub> ratio causes some fluctuation in the temperature at 4.9 cm, in the range between 467 °C and 501 °C after 10 min plasma reaction (Figure 6C). After 20 min, at the same positions, the reactions with higher CO<sub>2</sub> fractions had lower temperature differences with the measurements at 10 min, suggesting that more CO<sub>2</sub> present in the gas flow yields more stable temperatures. This is in accordance with the results in Figure 6A, where higher CO<sub>2</sub> fractions resulted in lower but more stable plasma temperatures.

Finally, upon H<sub>2</sub>O addition (Figure 6D), the temperature at 4.9 cm first slightly increases and then decreases once the H<sub>2</sub>O content is over 70% RH. This could be due to the high heat capacity of H<sub>2</sub>O, which adsorbs more heat. At 100% RH, as shown in Figure S6, the plasma was not stable anymore, leading to lower gas temperatures after the plasma in 10 min. Note that at 9.8 cm, with 40% RH, the temperature dropped from 427 °C to 380 °C (Figure 6D). The reason for this is however unclear.

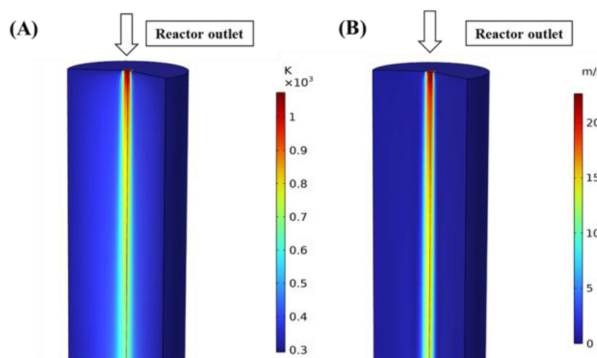
### Computational Results and Considerations for the Post-Plasma Catalyst Bed

Figure 7 shows the temperature profile in the GAP reactor as calculated by the 3D CFD model. The figure shows that the gas



**Figure 7.** Calculated gas temperature profile in the GAP reactor for a 1/1/8 CO<sub>2</sub>/CH<sub>4</sub>/N<sub>2</sub> gas mixture and a flow rate of 8 L/min.

temperature reaches values close to 3500 K in the center of the plasma, which is in line with the calculated gas temperatures for CO<sub>2</sub> and CH<sub>4</sub> plasmas in the GAP from previous work.<sup>[32,34]</sup> Once the gas reaches the outlet of the reactor, it has cooled down to a gas temperature of around 1100 K. Figure 8A shows the gas temperature profile beyond the GAP reactor in the post-plasma reactor tube, as calculated by the 2D axisymmetric CFD model. This profile shows how the gas cools down further as it leaves the reactor body and flows through the post-plasma reactor tube. From this profile it is clear that the heat of the exhaust gas is not transported evenly over the whole volume of the tube, but is concentrated in the center of the reactor. This is



**Figure 8.** (A) Calculated gas temperature profile and (B) calculated flow velocity profile in the post-plasma reactor tube for a 1/1/8 CO<sub>2</sub>/CH<sub>4</sub>/N<sub>2</sub> mixture gas mixture and a flow rate of 8 L/min.

attributed to the high gas flow velocity that is present as the gas flows out through the small reactor outlet, as demonstrated by the calculated gas flow velocity profile in Figure 8B. The high gas flow drags the heat along through convective heat transport, leaving no time for the gas to diffuse in the radial direction through conductive heat transport.

This has important implications for considering a post-plasma catalyst bed inside the tube, as catalysts located in the center of the tube will experience a significantly higher temperature compared to catalysts near the edge of the tube. As the activity, selectivity and stability of a catalyst are strongly dependent on the temperature, this is an important factor for the post-plasma catalyst process in combination with GAP reactors. For the implementation of a post-plasma catalyst bed, it could thus prove beneficial to disturb the centralized flow stream, by e.g. modifying the reactor outlet with a nozzle, introducing more gas mixing and/or more radial heat transport in the post-plasma tube. Introducing the catalyst bed in the tube will also, to some degree, already introduce some disturbance to the central flow stream. In addition, the experimental results (Figure 6 and Figure S3–S6) show a different temperature depending on the distance of the catalyst bed from the plasma exhaust. It should also be realized that the presence of a catalyst bed will alter the flow behavior and heat transfer,<sup>[35]</sup> thus necessitating further assessment of the temperature profile once a catalyst bed has been implemented. Nonetheless, our study of the post-plasma zone temperature profile without catalysts has already provided insights into how and where to implement the catalysts, laying a foundation for future studies. Finally, also the feed composition will have an influence on temperature and exhaust gas composition, as demonstrated by the above results and discussion in the temperature part, that can also affect the catalytic performance.

Figure 9 displays the axial temperature profile in the center of the post-plasma reactor tube, as calculated by the 2D axisymmetric CFD model, and compared to the thermocouple measurements shown in Figure 6, serving as a validation for the modelling results. While some deviation in absolute values is present and the trend is not the same, a decreasing temperature is observed in both the model and experiments. In

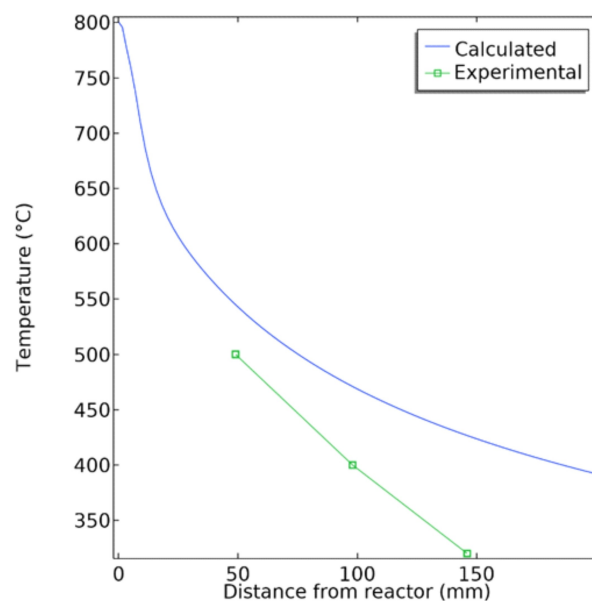


**Figure 9.** Comparison of temperature measured and modelled for the GAP reactor, as a function of distance from the reactor outlet, at a gas flow rate of 8 L/min and gas composition CO<sub>2</sub>/CH<sub>4</sub>/N<sub>2</sub> = 1/1/8.

general, these results can give us a better idea of where to place a post-plasma catalyst bed. Combined with the experimental results of thermal catalytic DRM,<sup>[44–46]</sup> which indicated that a temperature above 500 °C is necessary for the catalysts to show catalytic activity, we recommend that the distance of a post-plasma catalyst bed should be shorter than 4.9 cm. Considering the closer the distance from the plasma exhaust, the higher the temperature will be, as well as the possible backflow effect caused by the addition of a catalyst bed,<sup>[35]</sup> the distance of a post-plasma catalysis bed should be carefully investigated.

## Conclusions

We have experimentally investigated the impact of the addition of N<sub>2</sub>, N<sub>2</sub>/CH<sub>4</sub> (varying gas flow rate and CO<sub>2</sub>/CH<sub>4</sub> ratios), and N<sub>2</sub>/CH<sub>4</sub>/H<sub>2</sub>O on the CO<sub>2</sub> (and CH<sub>4</sub>) conversion, product selectivity and EC in a GAP. We also measured the temperature at three different distances from the plasma exhaust (4.9 cm, 9.8 cm, and 14.6 cm), and we calculated the temperature distribution inside the GAP and in the post-plasma reactor tube by computational fluid dynamics simulations, to provide insights for potential post-plasma catalyst applications.

### Generally, the Following Conclusions Can be Drawn

- (1) The addition of N<sub>2</sub> enhances the absolute conversion of CO<sub>2</sub> from 4% without N<sub>2</sub> to 13% with 80% N<sub>2</sub>, although the effective conversion decreases due to dilution of CO<sub>2</sub>. As a result of the latter, the EC increases significantly upon rising N<sub>2</sub> fraction. Considering that industrial gas emissions



contain significant amounts of N<sub>2</sub>, a mixture with 80% N<sub>2</sub> content, to achieve high absolute CO<sub>2</sub> conversion, is a reasonable choice, while lower N<sub>2</sub> contents may be more beneficial if the higher EC is the most critical parameter.

- (2) The addition of CH<sub>4</sub> in combination with N<sub>2</sub> results in a more complex situation. At fixed CO<sub>2</sub>/CH<sub>4</sub> ratio of 1, increasing the gas flow rate from 6 L/min to 12 L/min causes a drop in the CO<sub>2</sub> and CH<sub>4</sub> conversions, selectivity of C<sub>2</sub>H<sub>2</sub>, ratio of H<sub>2</sub>/CO and EC, while the selectivity of CO and H<sub>2</sub> shows an increasing trend. Moreover, the low gas flow rate of 6 L/min damaged the cathode. Increasing the CO<sub>2</sub>/CH<sub>4</sub> ratio from 0.6 to 1.67 resulted in an increase in the absolute conversion of CH<sub>4</sub>, while the absolute conversion of CO<sub>2</sub> decreased. However, the effective conversion of CH<sub>4</sub> and CO<sub>2</sub> exhibited opposite trends. Besides this, the selectivity of C<sub>2</sub>H<sub>2</sub>, the H<sub>2</sub>/CO ratio, SEI, and EC all decreased with increasing fraction of CO<sub>2</sub>. Considering the damage of the GAP device at too low flow rates, and the obtained results for CO<sub>2</sub> and CH<sub>4</sub> conversion, CO and H<sub>2</sub> selectivity, we believe that 8 L/min with CO<sub>2</sub>/CH<sub>4</sub>/N<sub>2</sub> = 1/1/8 is a quite optimal condition.
- (3) The addition of H<sub>2</sub>O suppressed the conversion of CO<sub>2</sub> and CH<sub>4</sub>, with a more pronounced effect on the former, leading to a decrease in the absolute CO<sub>2</sub> conversion from 55% at 0% RH to 22% at 100% RH. However, as the CH<sub>4</sub> conversion was less affected, this improved the H<sub>2</sub>/CO ratio from 1.45 to 2. Furthermore, the SEI and EC both decreased significantly when H<sub>2</sub>O was added (between 10 and 40% RH) but then increased as the amount of H<sub>2</sub>O increased. Thus, H<sub>2</sub>O addition can help to improve the H<sub>2</sub> production and decrease the EC, albeit at the expense of some CO<sub>2</sub> conversion, which both help to increase the produced H<sub>2</sub>/CO ratio. This is beneficial for the further processing of syngas into other chemicals. However, the amount of H<sub>2</sub>O addition should be carefully studied, as too much H<sub>2</sub>O will affect the plasma stability and the post-plasma temperature.
- (4) Our measured temperature data suggest that N<sub>2</sub> dilution above 60% will increase the outlet gas temperature. When adding N<sub>2</sub>/CH<sub>4</sub> or N<sub>2</sub>/CH<sub>4</sub>/H<sub>2</sub>O, no dramatic changes were observed, and the temperatures at three distances from the exhaust generally ranged between 470–520 °C at 4.9 cm, 370–440 °C at 9.8 cm, and 330–350 °C at 14.6 cm. In order to make optimal use of the heat produced by the plasma, for activating post-plasma catalysts, the catalyst bed should thus be placed quite close to the GAP reactor exhaust, dependent on the temperature required for the catalytic process. However, considering the catalyst stability and the effect of active sites sintering at too high temperature, the distance should also not be too close to avoid destroying the catalyst.
- (5) Our CFD simulations indicate that the exhaust gas temperature is not transported uniformly over the post-plasma reactor tube but is concentrated in the center. This is also important for considering a post-plasma catalyst bed. Moreover, the simulations confirmed the decreasing temperature with increasing distance from the plasma exhaust.

In summary, our paper provides valuable insights into selecting suitable reaction conditions to achieve higher CO<sub>2</sub> (and CH<sub>4</sub>) conversion, lower energy costs, and higher syngas production, also important for post-plasma catalysis, as the exhaust gas of the plasma serves as the feed gas for the post-plasma catalytic reaction. Furthermore, the measured and calculated temperature profiles offer valuable information to design and position a post-plasma catalyst bed, taking the temperature distribution and gradients over the post-plasma reactor tube into account, as well as the impact of gas composition (e.g. dilution) on the post-plasma temperature.

## Experimental and Computational Section

Details on the experimental setup and the computational description, the configurations for plasma reaction, gas products analysis, including how to correct for the gas expansion, the equations defined for conversion, product selectivities, yield, specific energy input and energy cost, and temperature data are provided in the Supporting Information

## Supporting Information

The detailed experimental, computational description and temperature data are provided in the Supporting Information.

## Author Contributions

Wencong Xu performed experiments, data analysis, experimental part writing- original draft and conceptualization. Senne Van Alphen performed computational modelling, computational part writing- original draft and conceptualization. Vladimir V. Galvita performed review, editing, and supervision. Vera Meynen performed writing, review, editing, conceptualization, funding and supervision. Annemie Bogaerts performed writing, review, editing, conceptualization, funding and supervision.

## Acknowledgements

We acknowledge the VLAIO Catalisti Moonshot project D2M and the VLAIO Catalisti transition project CO<sub>2</sub>PERATE (HBC.2017.0692) for financial support. We acknowledge Gilles Van Loon for his help to make the quartz and steel devices for the reactor. Vladimir V. Galvita also acknowledges a personal grant from the Research Fund of Ghent University (BOF; 01N16319).

## Conflict of Interests

The authors declare no conflict of interest.

## Data Availability Statement

The data that support the findings of this study are available from the corresponding author upon reasonable request.

**Keywords:** CO<sub>2</sub> conversion · Plasma · Gliding arc plasmatron · Temperature profiles · Computational modelling

- [1] F. Van der Ploeg, C. Withageny, *Rev. Environ. Econ. Policy* **2015**, *9*, 285–303.
- [2] “National Oceanic and Atmospheric Administration (NOAA) Global Monitoring Laboratory,” can be found under <https://gml.noaa.gov/ccgg/trends/>, **2023**.
- [3] J. Ashok, S. Pati, P. Hongmanorom, Z. Tianxi, C. Junmei, S. Kawi, *Catal. Today* **2020**, *356*, 471–489.
- [4] G. H. Gunasekar, K. Park, K. D. Jung, S. Yoon, *Inorg. Chem. Front.* **2016**, *3*, 882–895.
- [5] M. Liu, Y. Yi, L. Wang, H. Guo, A. Bogaerts, *Catalysts* **2019**, *9*, 275.
- [6] M. Pérez-Fortes, J. C. Schöneberger, A. Boulamanti, G. Harrison, E. Tzimas, *Int. J. Hydrogen Energy* **2016**, *41*, 16444–16462.
- [7] M. Aresta, A. Dibenedetto, A. Angelini, *Chem. Rev.* **2014**, *114*, 1709–1742.
- [8] A. Mustafa, B. G. Lougou, Y. Shuai, Z. Wang, H. Tan, *J. Energy Chem.* **2020**, *49*, 96–123.
- [9] S. Saeidi, S. Najari, F. Fazlollahi, M. K. Nikoo, F. Sefidkon, J. J. Klemeš, L. L. Baxter, *Renewable Sustainable Energy Rev.* **2017**, *80*, 1292–1311.
- [10] I. V. Yentekakis, P. Panagiotopoulou, G. Artemakis, *Appl. Catal. B* **2021**, *296*, 120210.
- [11] R. Snoeckx, A. Bogaerts, *Chem. Soc. Rev.* **2017**, *46*, 5805–5863.
- [12] M. Ramakers, G. Trenchev, S. Heijkers, W. Wang, A. Bogaerts, *ChemSusChem* **2017**, *10*, 2642–2652.
- [13] L. Di, J. Zhang, X. Zhang, *Plasma Processes Polym.* **2018**, *15*, e1700234.
- [14] G. Chen, R. Snyders, N. Britun, *J. CO<sub>2</sub> Util.* **2021**, *49*, 101557.
- [15] N. Anoop, S. Sundaramurthy, J. M. Jha, S. Chandrabalan, N. Singh, J. Verma, D. Parvatalu, S. Katti, *Clean Technol. Environ. Policy* **2021**, *23*, 2789–2811.
- [16] R. S. Abiev, D. A. Sladkovskiy, K. V. Semikin, D. Y. Murzin, E. V. Rebrov, *Catalysts* **2020**, *10*, 1358.
- [17] E. Suslova, S. Savilov, A. Egorov, A. Shumyantsev, V. Lunin, *Microporous Mesoporous Mater.* **2020**, *293*, 109807.
- [18] C. Wang, D. Li, Z. S. Lu, M. Song, W. Xia, *Chem. Eng. Sci.* **2020**, *227*, 115921.
- [19] W. C. Chung, M. B. Chang, *Renewable Sustainable Energy Rev.* **2016**, *62*, 13–31.
- [20] V. Palma, M. Cortese, S. Renda, C. Ruocco, M. Martino, E. Meloni, *Nanomaterials* **2020**, *10*, 1596.
- [21] S. Li, R. Ahmed, Y. Yi, A. Bogaerts, *Catalysts* **2021**, *11*, 590.
- [22] R. Aerts, W. Somers, A. Bogaerts, *ChemSusChem* **2015**, *8*, 702–716.
- [23] H. Kim, S. Song, C. P. Tom, F. Xie, *J. CO<sub>2</sub> Util.* **2020**, *37*, 240–247.
- [24] E. Cleiren, S. Heijkers, M. Ramakers, A. Bogaerts, *ChemSusChem* **2017**, *10*, 4025–4036.
- [25] T. Kozák, A. Bogaerts, *Plasma Sources Sci. Technol.* **2014**, *23*, 045004.
- [26] J. Feng, X. Sun, Z. Li, X. Hao, M. Fan, P. Ning, K. Li, *Adv. Sci.* **2022**, *9*, 1–36.
- [27] G. Trenchev, A. Bogaerts, *J. CO<sub>2</sub> Util.* **2020**, *39*, 101152.
- [28] Y. Wang, N. Wang, J. Harding, G. Chen, X. Tu, *Plasma Technology for Syngas Production*, Elsevier Inc., **2023**.
- [29] H. Sun, Z. Chen, J. Chen, H. Long, Y. Wu, W. Zhou, *J. Phys. D* **2021**, *54*, 495203.
- [30] H. Zhang, L. Li, X. Li, W. Wang, J. Yan, X. Tu, *J. CO<sub>2</sub> Util.* **2018**, *27*, 472–479.
- [31] F. Jardali, S. Van Alphen, J. Creel, H. Ahmadi Eshtehardi, M. Axelsson, R. Ingels, R. Snyders, A. Bogaerts, *Green Chem.* **2021**, *23*, 1748–1757.
- [32] G. Trenchev, S. Kolev, W. Wang, M. Ramakers, A. Bogaerts, *J. Phys. Chem. C* **2017**, *121*, 24470–24479.
- [33] J. Slaets, M. Aghaei, S. Ceulemans, S. Van Alphen, A. Bogaerts, *Green Chem.* **2020**, *22*, 1366–1377.
- [34] S. Van Alphen, J. Slaets, S. Ceulemans, M. Aghaei, R. Snyders, A. Bogaerts, *J. CO<sub>2</sub> Util.* **2021**, *54*, 101767.
- [35] H. Zhang, L. Li, R. Xu, J. Huang, N. Wang, X. Li, X. Tu, *Waste Dispos. Sustain. Energy* **2020**, *2*, 139–150.
- [36] Z. A. Allah, J. C. Whitehead, *Catal. Today* **2015**, *256*, 76–79.
- [37] J. L. Liu, Z. Li, J. H. Liu, K. Li, H. Y. Lian, X. S. Li, X. Zhu, A. M. Zhu, *Catal. Today* **2019**, *330*, 54–60.
- [38] M. Ramakers, S. Heijkers, T. Tytgat, S. Lenaerts, A. Bogaerts, *J. CO<sub>2</sub> Util.* **2019**, *33*, 121–130.
- [39] Y. Xia, N. Lu, N. Jiang, K. Shang, Y. Wu, *J. CO<sub>2</sub> Util.* **2020**, *37*, 248–259.
- [40] R. Snoeckx, A. Ozkan, F. Reniers, A. Bogaerts, *ChemSusChem* **2017**, *10*, 409–424.
- [41] F. Girard-Sahun, O. Biondo, G. Trenchev, G. van Rooij, A. Bogaerts, *Chem. Eng. J.* **2022**, *442*, 136268.
- [42] J. Ma, X. Chen, M. Song, C. Wang, W. Xia, *Diamond Relat. Mater.* **2021**, *117*, 108445.
- [43] Y. J. Liu, N. Cui, P. L. Jia, X. Wang, W. Huang, *ACS Sustainable Chem. Eng.* **2020**, *8*, 6634–6646.
- [44] X. Lin, R. Li, M. Lu, C. Chen, D. Li, Y. Zhan, L. Jiang, *Fuel* **2015**, *162*, 271–280.
- [45] D. Y. Kalai, K. Stangeland, Y. Jin, Z. Yu, *J. CO<sub>2</sub> Util.* **2018**, *25*, 346–355.
- [46] Z. Taherian, V. Shahed Gharahshiran, A. Khataee, Y. Orooji, *Fuel* **2022**, *311*, 122620.

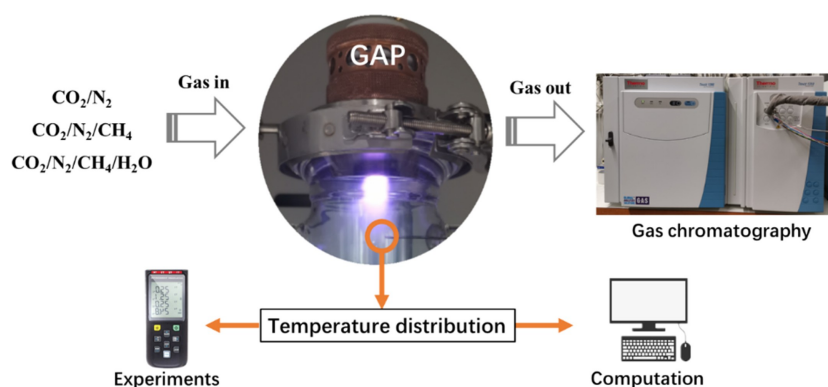
Manuscript received: January 25, 2024

Revised manuscript received: March 12, 2024

Accepted manuscript online: March 14, 2024

Version of record online: ■■■, ■■■

# RESEARCH ARTICLE



We illustrate the effect of adding  $\text{N}_2$ ,  $\text{N}_2/\text{CH}_4$  and  $\text{N}_2/\text{CH}_4/\text{H}_2\text{O}$  to a  $\text{CO}_2$  gliding arc plasmatron (GAP). Adding  $\text{N}_2$  and  $\text{CH}_4$  improves the  $\text{CO}_2$  conversion.  $\text{N}_2$  addition increases the tem-

perature at 4.9 cm post-plasma, while the  $\text{CO}_2/\text{CH}_4$  ratio has no significant effect. Our computational results confirm the decreasing trend of temperature after plasma.

W. Xu, S. Van Alphen, Prof. V. V. Galvita, Prof. V. Meynen, Prof. A. Bogaerts\*

1 – 11

**Effect of Gas Composition on Temperature and  $\text{CO}_2$  Conversion in a Gliding Arc Plasmatron reactor: Insights for Post-Plasma Catalysis from Experiments and Computation**

